# Beam Splitter and Boson Sampling

Jhih-Sheng Wu

2026

## Contents

Beam splitters are essential optical components that have a profound impact on both classical and quantum optics by dividing incoming light beams into reflected and transmitted parts. This note delves into their quantum mechanical behavior, illustrating how they manipulate light at the photon level. We begin by examining the classical description, where amplitudes split predictably, and then transition to quantum descriptions using annihilation operators to uncover uniquely quantum phenomena.

A key concept explored is the transformation of single-photon states, which leads to entangled outputs. This is notably demonstrated in the Mach-Zehnder interferometer, where quantum interference allows for precise measurements such as phase determination, with implications for quantum computing and sensing. We also investigate the Hong-Ou-Mandel effect, a striking example of quantum interference where two photons incident on a symmetric beam splitter exhibit "bunching" rather than the classically expected distribution. This non-classical result is fundamental to linear optical quantum computing. Furthermore, the note differentiates the outcomes for N-photon states, which become entangled after passing through a beam splitter, from coherent states, which remain unentangled.

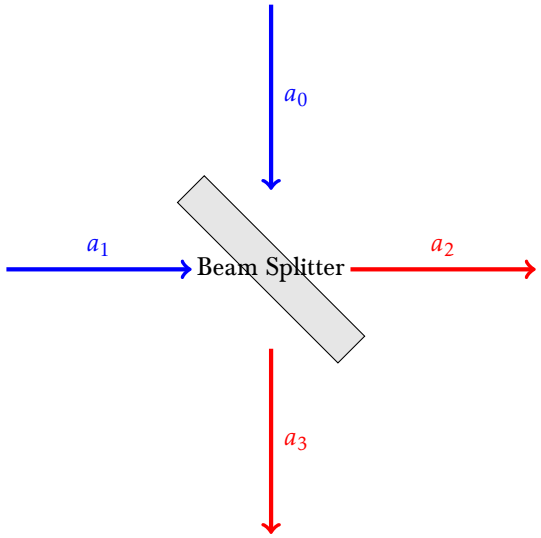


- Indistinguishability of boson

- Gaussian boson sampling

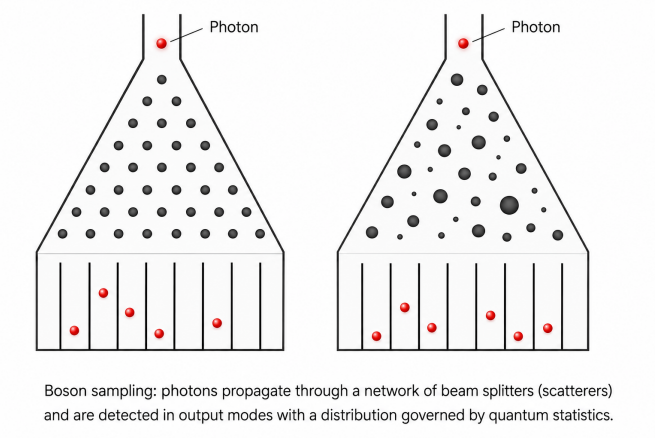


Figure 1: Play a Galton board with photons.

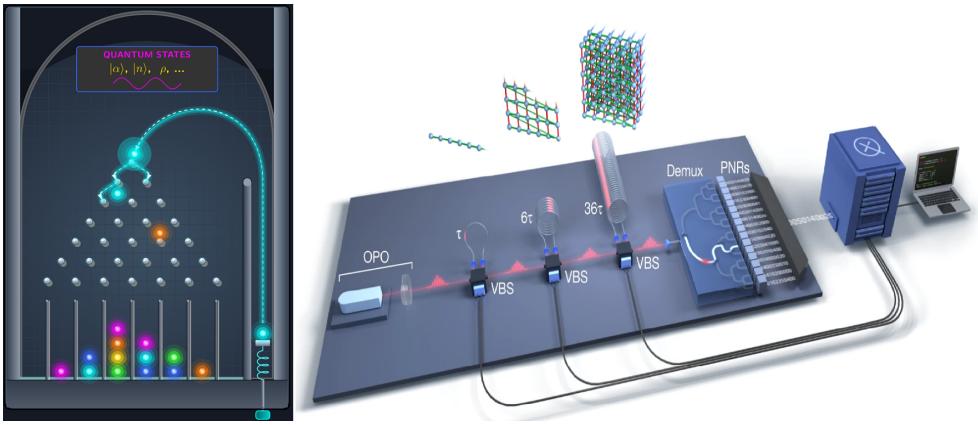


Figure 2: Quantum computation with a Galton board. Adapted from Ref. [3].

# 1 Recent Progress in Programmable Boson Sampling and Quantum Simulation

**Boson sampling in a nutshell.** At its heart, boson sampling can be pictured as a quantum version of Galton's bean machine (the "plinko" board). In the classical Galton board, balls are dropped through a lattice of pegs and bounce left or right at random, producing a binomial distribution in the output bins. In boson sampling, the balls are replaced by *indistinguishable single photons* and the pegs by a network of beam splitters and phase shifters that together implement a Haar-random unitary $U$ acting on $M$ optical modes. When $N$ photons are injected into selected input modes and photon-number detectors are placed at the outputs, the probability of observing a given click pattern is no longer governed by simple binomial statistics: it is proportional to $|\mathrm{Per}(U_S)|^2$, the squared modulus of the permanent of an $N \times N$ submatrix of $U$. Because quantum interference among the $N!$ indistinguishable photon paths cannot be factorized, and because computing matrix permanents is #P-hard, sampling from this distribution is believed to be classically intractable for $N \gtrsim 50$. In Gaussian Boson Sampling (GBS), the single photons are replaced by squeezed-vacuum states and the permanent by the closely related *hafnian*, which is exper-

imentally more scalable and underlies most current photonic quantum-advantage demonstrations. Boson sampling is therefore not a universal quantum computer, but rather a minimal, purely passive linear-optical experiment whose output statistics are conjectured to lie beyond the reach of any classical simulator—a "photon Galton board" designed specifically to expose the computational power of bosonic quantum interference.

Following the demonstration of quantum computational advantage with a programmable photonic processor in 2022 [3], the field has rapidly diversified. Below we summarize recent progress under four thematic headings.

## 1.1 Massive Hardware Scaling and Quantum Advantage

The race to enlarge photon number, mode count, and circuit programmability has produced several landmark systems. In late 2023, the USTC group deployed the *Jiuzhang 3.0* processor, which uses pseudo-photon-number-resolving (PPNR) detection based on time-bin demultiplexing and registers up to 255 photon-click events, dramatically increasing the cost of brute-force classical simulation [5]. In 2025, Xanadu's *Aurora* system pushed scaling in an orthogonal direction by interconnecting 35 photonic chips across four server racks through roughly 13 km of optical fiber, providing a room-temperature proof-of-principle for a *modular, networked* photonic quantum computer [6].

These experimental advances have been continuously stress-tested by sharper classical algorithms. Oh *et al.* introduced a tensor-network simulator that exploits realistic photon loss to reproduce the largest published GBS data sets with modest resources [7], while a separate analysis demonstrated that classical adversaries can also *spoof* the cross-entropy benchmarks used to certify GBS experiments [8]. Phase-space (positive-$P$) methods have been similarly developed into independent validation and simulation tools for noisy GBS data [9]. On the theory side, Go *et al.* analyzed shallow-depth boson sampling and proposed nonlocal linear-optical circuits that balance noise (which grows with depth) against classical simulability (which is harder at greater depth) [10], and established average-case #P-hardness of estimating output probabilities for logarithmic-depth boson sampling, providing complexity-theoretic support for noise-tolerant quantum advantage [11].

## 1.2 Breakthroughs in Quantum AI and Machine Learning

A second major thrust has been to repurpose boson sampling hardware as a co-processor for machine learning. Hoch *et al.* demonstrated quantum machine learning protocols on a universal programmable photonic circuit by introducing post-selection-based adaptivity, allowing dimension-enhanced classification within a linear-optical platform [12]. In parallel, GBS-assisted *unsupervised* learning has been experimentally demonstrated on a universal photonic chip, with photon-click statistics serving as a quantum-enhanced feature map for clustering tasks [13]. A more recent proposal uses GBS within an extreme learning machine architecture for image recognition, harnessing the high-dimensional Hilbert space of photon-click

patterns as a fixed, nonlinear reservoir [14]. These developments connect directly to the broader research program of using GBS-generated graph kernels and subgraph-sampling statistics as quantum features for structured-data learning [15].

### 1.3 Deeper Convergence with Quantum Chemistry

The original chemistry motivation of Huh *et al.*—using boson sampling to simulate Franck–Condon factors and molecular vibronic spectra [4]—has matured into a more careful study of *where* a genuine quantum advantage in chemistry is to be expected. A linear-coupling-model algorithm benchmarked on pentacene clarifies which vibronic transitions plausibly demand quantum hardware acceleration and which remain classically tractable [16]. A complementary analysis explicitly delineates the boundary between molecules that genuinely require a GBS treatment (e.g., those with strong Duschinsky mode mixing or significant anharmonicity) and those for which classical algorithms remain competitive [17]. Together, these works mark a shift from "GBS can in principle solve vibronic problems" to a more granular, application-driven assessment of quantum chemistry use cases.

### 1.4 Advanced Hybrid and Nonlinear Models

Finally, to escape the practical limits of purely passive, linear-optical sampling, researchers are increasingly exploring *hybrid* architectures that combine boson sampling with other quantum modalities. A recent comprehensive review surveys photonic hybrid quantum computing, in which discrete-variable (single-photon) qubits are entangled with continuous-variable (squeezed or cat-like) bosonic modes to enable near-deterministic gates, measurement-based computation, and substantially improved loss thresholds [18]. On the analog-simulation side, the convergence of large-scale quantum hardware with error correction has been most dramatically demonstrated in a complementary platform: Bluvstein *et al.* executed algorithms on up to 48 logical, error-corrected qubits in a reconfigurable neutral-atom array of 280 physical qubits [19]. While this latter result is not a boson-sampling experiment, it establishes the kind of programmable, logically protected simulator toward which photonic platforms—through nonlinear elements, adaptivity, and hybrid encodings—are now actively converging.

## 2 Beam Splitters

A beam splitter is an optical component that is partially transparent. An incident beam on a beam splitter is partially reflected and partially transmitted, splitting into two beams. Classically, an incident beam with an amplitude $A_1$ is split into a reflected beam with the amplitude $A_1$ and a transmitted beam with the amplitude $A_2$. The amplitudes are related by the coefficients of reflection and transmission,

$$A_2 = rA_1, \tag{2.1}$$

$$A_3 = tA_1. \tag{2.2}$$

We can also consider another case in which a beam of amplitude $A_0$ is incident on the other side of the beam splitter. In this case, the amplitudes are related by

$$A_2 = t'A_0, \tag{2.3}$$
$$A_3 = r'A_0. \tag{2.4}$$

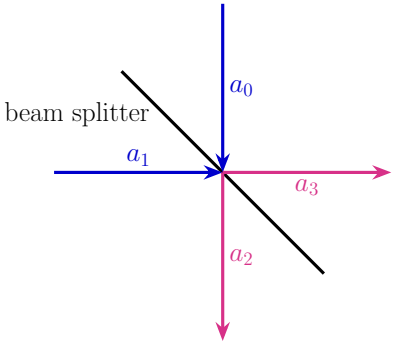


Figure 3: Beam splitter. Quantum descriptions where the annihilation operators replace the amplitudes.

The scattering matrix describes a beam splitter

$$\begin{pmatrix} A_2 \\ A_3 \end{pmatrix} = \begin{pmatrix} t' & r \\ r' & t \end{pmatrix} \begin{pmatrix} A_0 \\ A_1 \end{pmatrix} \equiv U \begin{pmatrix} A_0 \\ A_1 \end{pmatrix}. \tag{2.5}$$

Because of energy conservation, the matrix $U$ must be unitary so that

$$|r|^2 + |t|^2 = 1 \tag{2.6}$$
$$|r'|^2 + |t'|^2 = 1 \tag{2.7}$$
$$tr^* + t'^* r' = 0. \tag{2.8}$$

In order to satisfy Eq. (2.8), the phase of each beam cannot be arbitrary. Let's consider the example of a symmetric beam splitter. Let the phase between $r$ and $t$ is $\theta$ , that is, $\mathrm{Arg}\left[\frac{t}{r}\right] = \theta$. A symmetric beam splitter implies $\mathrm{Arg}\left[\frac{t'}{r'}\right] = \theta$. Eq. (2.8) becomes

$$|r||t|\left(e^{i\theta} - e^{-i\theta}\right) = 0, \tag{2.9}$$

which gives $\theta = \pm\frac{\pi}{2}$. A discussion about the phases can be found in the Ref. [1].

The quantum description of a beam splitter is to replace amplitudes with annihilation operators. Let the right-going photons have the annihilation operator $a_1$, and the bottom-going photons have the annihilation operator $a_0$. The scattering matrix describes a beam splitter

$$\begin{pmatrix} a_2 \\ a_3 \end{pmatrix} = \begin{pmatrix} t' & r \\ r' & t \end{pmatrix} \begin{pmatrix} a_0 \\ a_1 \end{pmatrix} = U \begin{pmatrix} a_0 \\ a_1 \end{pmatrix}, \tag{2.10}$$
$$\begin{pmatrix} a_0 \\ a_1 \end{pmatrix} = \begin{pmatrix} t'^* & r' \\ r^* & t^* \end{pmatrix} \begin{pmatrix} a_2 \\ a_3 \end{pmatrix} = U^\dagger \begin{pmatrix} a_2 \\ a_3 \end{pmatrix}. \tag{2.11}$$

The incident beams, $a_0$ and $a_1$, are treated as two independent modes with the commutation relations

$$[a_0, a_0^\dagger] = 1, \tag{2.12}$$
$$[a_1, a_1^\dagger] = 1, \tag{2.13}$$
$$[a_0, a_1^\dagger] = 0. \tag{2.14}$$

From Eqs. (2.12), (2.13), (2.14), and (2.10), one can show that the operators $a_2$ and $a_3$ automatically satisfy

$$[a_i, a_j^\dagger] = \delta_{ij}. \tag{2.15}$$

Physically, these relations mean that after a beam splitter, a beam is split into two independent modes $a_2$ and $a_3$.

Below, we will discuss what happens to a quantum light after passing a beam splitter. We will consider the cases of a single photon state, $N$-photon state, and a coherent state. We will see that the Fock states exhibit quantum natures, where the output states are entangled, while the output state of a coherent state can be factorized.

## 2.1 Single Photon

The incident state $|0\rangle_0|1\rangle_1$ can be expressed as

$$|0\rangle_0|1\rangle_1 = a_1^\dagger|0\rangle_0|0\rangle_1. \tag{2.16}$$

From Eq. (2.11), the creation operators $a_0^\dagger$ and $a_1^\dagger$ are related to $a_2^\dagger$ and $a_3^\dagger$ by

$$\begin{pmatrix} a_0^\dagger \\ a_1^\dagger \end{pmatrix} = U^T \begin{pmatrix} a_2^\dagger \\ a_3^\dagger \end{pmatrix}. \tag{2.17}$$

After incidence on the beam splitter, the state becomes

$$U^T a_1^\dagger|0\rangle_0|0\rangle_1 = (ra_2^\dagger + ta_3^\dagger)|0\rangle_2|0\rangle_3 \tag{2.18}$$
$$= r|1\rangle_2|0\rangle_3 + t|0\rangle_2|1\rangle_3, \tag{2.19}$$

which is an entangled state.

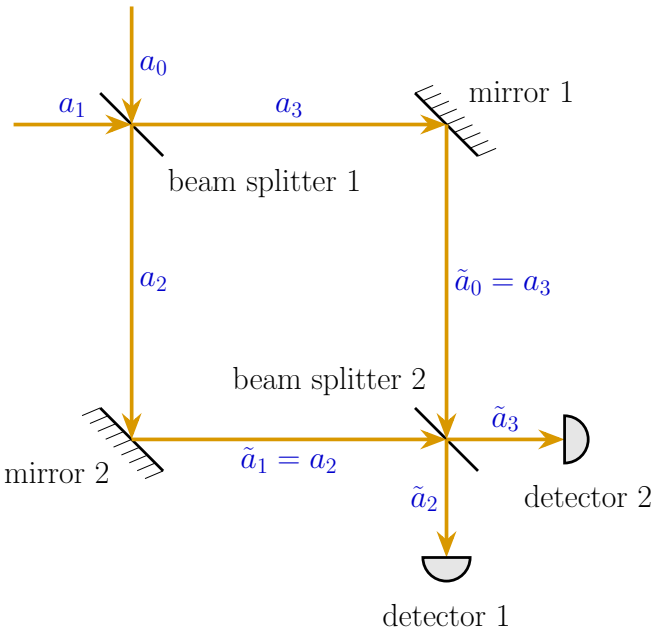


Figure 4: Mach–Zehnder interferometer.

Consider a Mach–Zehnder interferometer with two 50:50 beam splitters of $r = \frac{i}{\sqrt{2}}$ and $t = \frac{1}{\sqrt{2}}$. Let the initial state be $|0\rangle_0|1\rangle_1$. After the first beam splitter, the state becomes

$$\frac{i}{\sqrt{2}}|1\rangle_2|0\rangle_3 + \frac{1}{\sqrt{2}}|0\rangle_2|1\rangle_3. \tag{2.20}$$

When the state arrives at the second beam splitter, the state becomes

$$\frac{i}{\sqrt{2}}|1\rangle_2|0\rangle_3 + \frac{e^{i\theta}}{\sqrt{2}}|0\rangle_2|1\rangle_3, \tag{2.21}$$

where $\theta$ is a phase shift due to the difference of the two paths.

To deal with the second beam splitter, we first rename the modes. Modes 2 ($a_2$) and 3 ($a_3$) in the Eq. (2.21) become the incident beams to the second beam splitter. We rename Mode 2 ($a_2$) as the new Mode 1 ($\tilde{a}_1$) since it is right-going and Mode 3 ($a_3$) as the new Mode 0 ($\tilde{a}_0$) since it is bottom-going. For simplicity, we skip the tilde signs below. Now, we can use the same scattering matrix to find the final state after the second beam splitter,

$$\begin{pmatrix} a_2^\dagger \\ a_3^\dagger \end{pmatrix} = \begin{pmatrix} \frac{1}{\sqrt{2}} & \frac{i}{\sqrt{2}} \\ \frac{i}{\sqrt{2}} & \frac{1}{\sqrt{2}} \end{pmatrix} \begin{pmatrix} \frac{e^{i\theta}}{\sqrt{2}} a_0^\dagger \\ \frac{i}{\sqrt{2}} a_1^\dagger \end{pmatrix} \tag{2.22}$$

$$= \begin{pmatrix} \frac{(e^{i\theta}-1)}{2} a_0^\dagger \\ \frac{i(e^{i\theta}+1)}{2} a_1^\dagger \end{pmatrix} \tag{2.23}$$

The probability at $D_1$ is $\left|\frac{(e^{i\theta}-1)}{2}\right|^2 = \sin^2\frac{\theta}{2}$. The probability at $D_2$ is $\left|\frac{i(e^{i\theta}+1)}{2}\right|^2 = \cos^2\frac{\theta}{2}$. This is a more rigorous description of single-photon interference.

## 2.2 Two-Photon Hong-Ou-Mandel Effect

The Hong-Ou-Mandel effect is a simple but novel phenomenon of quantum optics. It is an example where quantum interference leads to a non-classical result. Consider a symmetric beam 50-50 beam splitter. Now, two single-photon states hit the beam splitter from different sides. As shown in Fig. 5, the initial state is $|1\rangle_0|1\rangle_1$. What will be the output state? Since the total input photon number is two, the output state could be $|2\rangle_2|0\rangle_3$, $|0\rangle_2|2\rangle_3$, and $|1\rangle_2|1\rangle_3$. Here, the subscripts of the ket denote on which side the photon state is, as in Fig. 5. Hence, a general expression for the output state is the superposition of the above possible states,

$$|\text{output}\rangle = \alpha|2\rangle_2|0\rangle_3 + \beta|0\rangle_2|2\rangle_3 + \gamma|1\rangle_2|1\rangle_3. \tag{2.24}$$

From the classical point of view, the state $|1\rangle_2|1\rangle_3$ seems the most possible state. However, in 1987, Hong et al. showed that for a symmetric beam splitter, $\gamma = 0$, that is, the probability of the state $|1\rangle_2|1\rangle_3$ is zero [2]. Specifically, the output state is

$$\begin{aligned}
|\text{output}\rangle &= U^T a_0^\dagger|0\rangle U^T a_1^\dagger|0\rangle && (2.25)\\
&= \begin{pmatrix} \frac{1}{\sqrt{2}} & \frac{i}{\sqrt{2}} \\ \frac{i}{\sqrt{2}} & \frac{1}{\sqrt{2}} \end{pmatrix} \begin{pmatrix} a_0^\dagger \\ 0 \end{pmatrix} \begin{pmatrix} \frac{1}{\sqrt{2}} & \frac{i}{\sqrt{2}} \\ \frac{i}{\sqrt{2}} & \frac{1}{\sqrt{2}} \end{pmatrix} \begin{pmatrix} 0 \\ a_1^\dagger \end{pmatrix} |0\rangle && (2.26)\\
&= \frac{1}{2}\left(a_2^\dagger + ia_3^\dagger\right)\left(ia_2^\dagger + a_3^\dagger\right)|0\rangle && (2.27)\\
&= \frac{i}{2}\left[\left(a_2^\dagger\right)^2 + \left(a_3^\dagger\right)^2\right]|0\rangle && (2.28)\\
&= \frac{i}{\sqrt{2}}(|2\rangle_2|0\rangle_3 + |0\rangle_2|2\rangle_3) && (2.29)
\end{aligned}$$

Surprisingly, two identical single photons are bunched after hitting a beam splitter from different sides. In the linear optical quantum computing, the Hong-Ou-Mandel effect is the mechanism for the logic gates.

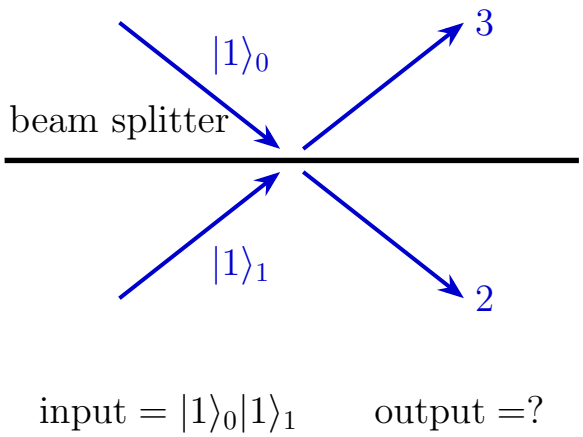


Figure 5: Hong-Ou-Mandel effect.

## 2.3 N-Photon

Let the initial state be $|0\rangle_0|N\rangle_1 = \frac{(a_1^\dagger)^N}{\sqrt{N!}}|0\rangle$. After a beam splitter, the state becomes

$$\frac{(Ua_1^\dagger)^N}{\sqrt{N!}}|0\rangle = \frac{(ta_2^\dagger + ra_3^\dagger)^N}{\sqrt{N!}}|0\rangle. \tag{2.30}$$

## 2.4 Coherent States

Let the initial state be $|0\rangle_0|\alpha\rangle_1 = D_1[\alpha]|0\rangle = e^{\alpha a_1^\dagger - \alpha^* a_1}|0\rangle$. After a beam splitter, the state becomes

$$\begin{aligned} e^{\alpha U a_1^\dagger - \alpha^* U^\dagger a_1}|0\rangle &= e^{\alpha t a_2^\dagger - \alpha^* t^* a_2} e^{\alpha r a_3^\dagger - \alpha^* r^* a_3}|0\rangle && (2.31)\\ &= D_2[t\alpha]D_3[r\alpha]|0\rangle && (2.32)\\ &= |t\alpha\rangle_2|r\alpha\rangle_3. && (2.33) \end{aligned}$$

The input of a coherent state is split into a product of two coherent states. Unlike the single-photon case, this state is not entangled.

Consider a Mach–Zehnder interferometer with two 50:50 beam splitters of $r = \frac{i}{\sqrt{2}}$ and $t = \frac{1}{\sqrt{2}}$. Let the initial state be $|0\rangle_0|\alpha\rangle_1$. After the first beam splitter, the state becomes

$$\left|\frac{i\alpha}{\sqrt{2}}\right\rangle_2 \left|\frac{\alpha}{\sqrt{2}}\right\rangle_3. \tag{2.34}$$

When the state arrives at the second beam splitter, the state becomes

$$\left|\frac{i\alpha}{\sqrt{2}}\right\rangle_2 \left|\frac{e^{i\theta}\alpha}{\sqrt{2}}\right\rangle_3. \tag{2.35}$$

where $\theta$ is a phase shift due to the difference of the two paths. The final state after the second beam splitter is (see the figure: $a_2$ is the new $a_1$ and $a_3$ is the new $a_0$)

$$\left|\frac{\left(e^{i\theta}-1\right)}{2}\right\rangle_2 \left|\frac{i\left(e^{i\theta}+1\right)}{2}\right\rangle_3. \tag{2.36}$$

The intensity at $D_1$ is $|\alpha|^2\left|\frac{e^{i\theta}-1}{2}\right|^2 = \sin^2\frac{\theta}{2}|\alpha|^2$. The intensity at $D_2$ is $|\alpha|^2\left|\frac{e^{i\theta}+1}{2}\right|^2 = \cos^2\frac{\theta}{2}|\alpha|^2$. The two output beams are both coherent states. Thus, the phase $\theta$ can be obtained by

$$\frac{I_2 - I_1}{|\alpha|^2} = \cos\theta. \tag{2.37}$$

However, the amplitudes have uncertainty $\sigma(n) = \sqrt{\bar{n}}$. Thus, the phase has the uncertainty $\sigma(\theta) \sim \frac{1}{\sqrt{\bar{n}}}$. In experiments, we would like to use a coherent light (laser) with a well-defined phase and a strong intensity such that the uncertainty in the phase is small. However, a strong-intensity light may lead to more noise, such as radiation pressures, thermal noises, etc. To solve this dilemma, lights with small $\sigma(n)$ are used. These lights are non-classical lights.

# References


[1] Z. Y. Ou and L. Mandel, Derivation of reciprocity relations for a beam splitter from energy balance, American Journal of Physics 57, 66 (1989)

[2] C. K. Hong; Z. Y. Ou & L. Mandel . "Measurement of subpicosecond time intervals between two photons by interference." Phys. Rev. Lett. 59 (18): 2044–2046 (1987)

[3] Madsen, L. S., Laudenbach, F., Askarani, M. F., *et al.* (2022). Quantum computational advantage with a programmable photonic processor. *Nature*, 606(7912), 75–81. https://doi.org/10.1038/s41586-022-04725-x

[4] Huh, J., Guerreschi, G. G., Peropadre, B., McClean, J. R., & Aspuru-Guzik, A. (2015). Boson sampling for molecular vibronic spectra. *Nature Photonics*, 9(9), 615–620. https://doi.org/10.1038/nphoton.2015.153

[5] Deng, Y.-H., Gu, Y.-C., Liu, H.-L., *et al.* (2023). Gaussian Boson Sampling with Pseudo-Photon-Number-Resolving Detectors and Quantum Computational Advantage. *Physical Review Letters*, 131(15), 150601. https://doi.org/10.1103/PhysRevLett.131.150601

[6] Aghaee Rad, H., Ainsworth, T., Alexander, R. N., *et al.* (2025). Scaling and networking a modular photonic quantum computer. *Nature*, 638, 912–919. https://doi.org/10.1038/s41586-024-08406-9

[7] Oh, C., Liu, M., Alexeev, Y., Fefferman, B., & Jiang, L. (2024). Classical algorithm for simulating experimental Gaussian boson sampling. *Nature Physics*, 20, 1461–1468. https://doi.org/10.1038/s41567-024-02535-8

[8] Oh, C., Jiang, L., & Fefferman, B. (2023). Spoofing Cross-Entropy Measure in Boson Sampling. *Physical Review Letters*, 131(1), 010401. https://doi.org/10.1103/PhysRevLett.131.010401

[9] Drummond, P. D., Dellios, A. S., Reid, M. D., *et al.* (2025). Validation tests of GBS quantum computers give evidence for quantum advantage with a decoherent target. *Physics Letters A*, 543, 130459. https://doi.org/10.1016/j.physleta.2025.130459

[10] Go, B., Oh, C., Jiang, L., & Jeong, H. (2024). Exploring shallow-depth boson sampling: Toward a scalable quantum advantage. *Physical Review A*, 109(5), 052613. https://doi.org/10.1103/PhysRevA.109.052613

[11] Go, B., Oh, C., & Jeong, H. (2024). On computational complexity and average-case hardness of shallow-depth boson sampling. *arXiv preprint*, arXiv:2405.01786. https://doi.org/10.48550/arXiv.2405.01786

[12] Hoch, F., Rodari, G., Giordani, T., *et al.* (2025). Quantum machine learning with Adaptive Boson Sampling via post-selection. *Nature Communications*, 16, 902. https://doi.org/10.1038/s41467-025-55877-z

[13] Zhang, M., Wang, Y., Pan, D., *et al.* (2024). GBS-Assisted Quantum Unsupervised Machine Learning on a Universal Photonic Processor. *Research*, 7, 1006. https://doi.org/10.34133/research.1006

[14] Li, J., *et al.* (2025). Enhanced Image Recognition Using Gaussian Boson Sampling. *arXiv preprint*, arXiv:2506.19707. https://doi.org/10.48550/arXiv.2506.19707

[15] Schuld, M., Brádler, K., Israel, R., Su, D., & Gupt, B. (2020). Measuring the similarity of graphs with a Gaussian boson sampler. *Physical Review A*, 101(3), 032314. https://doi.org/10.1103/PhysRevA.101.032314

[16] Konyshev, I., *et al.* (2025). Calculating Vibronic Spectra with a linear algorithm based on Gaussian Boson Sampling. *arXiv preprint*, arXiv:2508.03943. https://doi.org/10.48550/arXiv.2508.03943

[17] Jnane, H., *et al.* (2025). Bridging chemistry and Gaussian boson sampling: A photonic alternative for vibronic spectra. *arXiv preprint*, arXiv:2507.19442. https://doi.org/10.48550/arXiv.2507.19442

[18] Lee, S.-W., Omkar, S., Jeong, H., *et al.* (2025). Photonic hybrid quantum computing. *Newton*, in press; also available as arXiv:2510.00534. https://doi.org/10.48550/arXiv.2510.00534

[19] Bluvstein, D., Evered, S. J., Geim, A. A., *et al.* (2024). Logical quantum processor based on reconfigurable atom arrays. *Nature*, 626(7997), 58–65. https://doi.org/10.1038/s41586-023-06927-3